Gating Mechanisms of Mechanosensitive Channels of Large Conductance, II: Systematic Study of Conformational Transitions

Yuye Tang,* Jejoong Yoo,† Arun Yethiraj,† Qiang Cui,† and Xi Chen*
*Nanomechanics Research Center, Department of Civil Engineering and Engineering Mechanics, Columbia University, New York, New York 10027; and †Theoretical Chemistry Institute, Department of Chemistry, University of Wisconsin, Madison, Wisconsin 53706

ABSTRACT Part II of this study is based on the continuum mechanics-based molecular dynamics-decorated finite element method (MDeFEM) framework established in Part I. In Part II, the gating pathways of *Escherichia coli*-MscL channels under various basic deformation modes are simulated. Upon equibiaxial tension (which is verified to be the most effective mode for gating), the MDeFEM results agree well with both experiments and all-atom simulations in literature, as well as the analytical continuum models and elastic network models developed in Part I. Different levels of model sophistication and effects of structural motifs are explored in detail, where the importance of mechanical roles of transmembrane helices, cytoplasmic helices, and loops are discussed. The conformation transitions under complex membrane deformations are predicted, including bending, torsion, cooperativity, patch clamp, and indentation. Compared to atom-based molecular dynamics simulations and elastic network models, the MDeFEM framework is unusually well-suited for simulating complex deformations at large length scales. The versatile hierarchical framework can be further applied to simulate the gating transition of other mechanosensitive channels and other biological processes where mechanical perturbation is important.

INTRODUCTION

To realize the function of a particular biomolecule, ''functional motions'' with specific characters (in direction, magnitude, and timescale) are induced in response to certain stimuli. Despite their biological importance, functional motions are difficult to identify and characterize at a quantitative level. The multiple length and timescales spanned by these motions pose tremendous challenges to experimental measurements and their interpretation (1). Careful computational studies can nicely complement experimental work for better characterizing and understanding the working mechanism of functional motions.

An interesting example of functional motion is the gating transition of mechanosensitive channels of large conductance (MscL), which act as the ''safety valve'' for bacteria by opening up as osmotic pressure goes above a certain threshold (2,3). MscL is one of the first examples that illustrated that mechanical sensing can occur without the involvement of cytoskeleton (4); the sensing process occurs through the mechanical deformation of the lipid membrane and its interaction with the embedded protein, although a complete understanding of the gating mechanism is not yet available due in part to the challenges mentioned above.

In Part I of this study, a theoretical and computational framework based on the molecular dynamics-decorated finite element method (MDeFEM) is described. The continuum mechanics-based protocol is aimed to effectively extend the length scales and timescales of the functional motions of biomolecules that can be simulated while retaining essential physical features derived from atomistic studies. Specifically, the MDeFEM simulation propagates information from all-atom simulations to an effective coarse-grained level based on continuum mechanics, which then can be used with finite element analysis to study the conformational response of the biomolecule to external mechanical perturbation. As already emphasized in Part I, although the parameterization procedure can be very elaborate using sophisticated all-atom molecular dynamics simulations, we limit ourselves in this study to simple parameterizations using molecular mechanics-based energy scan and normal mode calculations so that we can focus on the most fundamental physical principles that govern MscL gating.

In Part II, we use the MDeFEM approach to systematically analyze the gating behavior of MscL under diverse mechanical deformations of the surround membrane. The MDeFEM simulations are compared with all-atom simulations (5), the structural model (6), and experiment (7), as well as the analytical models established in Part I, to evaluate the effectiveness of the top-down hierarchical numerical approach and the simple analytical solutions, and to identify the most important gating factors, including the sensitivity of MscL toward various basic loading modes, the effects of different structural motifs, and cooperativity of neighboring MscLs. These numerical experiments can potentially not only help elucidate gating mechanisms but also stimulate new experiments for mechanistic analysis.

Most results presented in this article, in particular the snapshots of protein conformations during the transitions and the evolution of the effective pore radius (defined in Part I), are presented as functions of the fractional time, which is a progressive variable with $t = 0$ corresponding to the closed state, $t = 1.0$ for the maximum load and a linear variation in between.

Submitted December 27, 2007, and accepted for publication March 18, 2008.

Address reprint requests to Xi Chen, Tel.: 212-854-3787; Fax: 212-854-6267; E-mail: xichen@civil.columbia.edu.

Editor: Ron Elber.

0006-3495/08/07/581/16 $2.00

doi: 10.1529/biophysj.107.128496

GATING MECHANISMS UNDER EQUIBIAXIAL TENSION

Equibiaxial tension is believed to be the most relevant and effective loading mode on the membrane for the function of MscL; it can occur when the osmotic pressure in the cell is varied. Therefore, it is also the most studied mode in the literature. In addition to elucidating the gating mechanisms and comparing with previous modeling efforts (5,6,8), we explore how different levels of continuum model and various structural motifs would affect gating. In fact, this is an advantage of computational studies, since certain components can be easily taken off or shielded during simulation so as to explore their effects, which is difficult to do with a lab experiment.

Conformational transition

The assembled MDeFEM model (see Part I for details) of *Escherichia coli*-MscL (*E. coli*-MscL) under equibiaxial tension is given in Fig. 1 *a* (a zoomed-in view near the protein); the actual membrane size is much larger than that depicted in Fig. 1 *a* and much larger than the protein dimension. An equibiaxial membrane strain $\varepsilon_m = \bar{\sigma}(1 - \bar{\nu}_t)/\bar{E}_t$ (up to 21%) is applied as a displacement boundary condition on the perimeter of the membrane. (Due to the limitation of the elastic solid slab model used for lipid in this article, such membrane strain of about 20% is unrealistic and would rupture the membrane. Nevertheless, we focus on the conformational transition of the MscL in this article, and despite its bias, the current lipid model can effectively describe the appropriate expansion of lipid cavity that is needed to accommodate the full gating of MscL upon equibiaxial tension, which is essential for revealing essential aspects of the gating process (see details below). Further improvements that can reduce the level of membrane stress needed for gating are discussed later in the section, ''Limitations of the current implementation''.) Here, $\bar{\sigma}$ is the averaged stress across thickness according to the rule of mixture, and $\bar{E}_t$ and $\bar{\nu}_t$ are the equivalent Young's modulus and Poisson's ratio of the entire lipid bilayer (see the ''In-plane tension'' subsection in Part I). The snapshots of the channel at $t = 0.5$ and 1.0 are given in Fig. 1 *b* and compared to the structural model (6) for both the top and side views.

The most notable conformation transitions lie in the transmembrane region. As ε_m is increased, the expanding lipid cavity primarily pulls the TM2 bundle open via nonbonded attraction (although it also exerts smaller force on the TM1 helices). The TM1 pore is also pulled open in part due to its direct interaction with the lipid cavity; and in part due to the TM2-TM1 interactions, the effective pore radius is increased. Besides radial expansion, the TM/TM2 helices also tilt during the gating process. Before deformation, the top of the TM1 helix (also referred to as S2) and the bottom of the TM2 helix protrude outside of the membrane; with tilting, both tips move into the transmembrane region by the end of the gating transition. The tilting of the TM1 helix bundle is more significant than that of the TM2 bundle since the former is longer and more flexible. The simulation also shows that the transmembrane helices are highly elastic and deformable, and they are significantly stretched and bent to maintain mechanical equilibrium during the gating process; to our knowledge, this has not been shown in any experimental studies so far due to the limitation in resolution (although the structural model (6) has at least qualitatively shown the similar helix bending curvature, as compared in Fig. 1 *b*). Whether the magnitude of these effects is overestimated by the current model remains to be further analyzed.

Other protein components are also involved during the gating transition: the loops connecting TM1 and TM2 helices impose constraints on the sizes of the pore (see below). Due to the strong interactions between TM1 and S1 helices as well as through the loops connecting them, the S1 helices become more horizontal and are lifted up toward the transmembrane region; in addition, the S1 expands radially, which leads to an increment of the pore formed by the S1 bundle (whose size is comparable with the TM1 pore). Due to the loops that connect the TM2 and S3 helices, the S3 helices move upward and the pore enclosed by the S3 helix bundle also enlarges slightly; the orientation of S3 helices, however, is essentially unchanged. The protein conformational transitions discussed above are reversible once the load is removed.

For both half-opened and fully opened configurations, the MDeFEM simulation results are in good qualitative agreement with the structural model (6), especially regarding the orientation, displacement, and curvature of the deformed transmembrane helices. This demonstrates the effectiveness of the continuum model. The main difference is that the expansion of the pore enclosed by the S1 helices is smaller in the structural model; this may be due in part to the neglect of solvation effects in the current model.

We note that in a previous version of the structural model (8), the S3 helices are lifted up into the membrane and become horizontal in the open state, playing an indispensable role during the gating process. In a later model (6), however, the S3 helices are essentially static during gating. Interestingly, the current simulation supports the newer structural model (6) and shows that the S3 helices are essentially unresponsive during the gating transition.

Pore radius evolution

The increment ratio of the effective pore radius calculated from MDeFEM is presented as a function of ε_m in Fig. 2 *a* (*solid-circle curve*). The pore radius increases almost monotonically with strain, and the iris-like features are due to the many-body interactions that affect equilibrium via helix stretching-relaxing cycles. Recall that in elasticity, the relationship between membrane tension and the lipid hole radius is linear (''In-plane tension'' subsection in Part I); thus the evolution of the pore radius and that of the membrane hole are expected to be closely coupled.

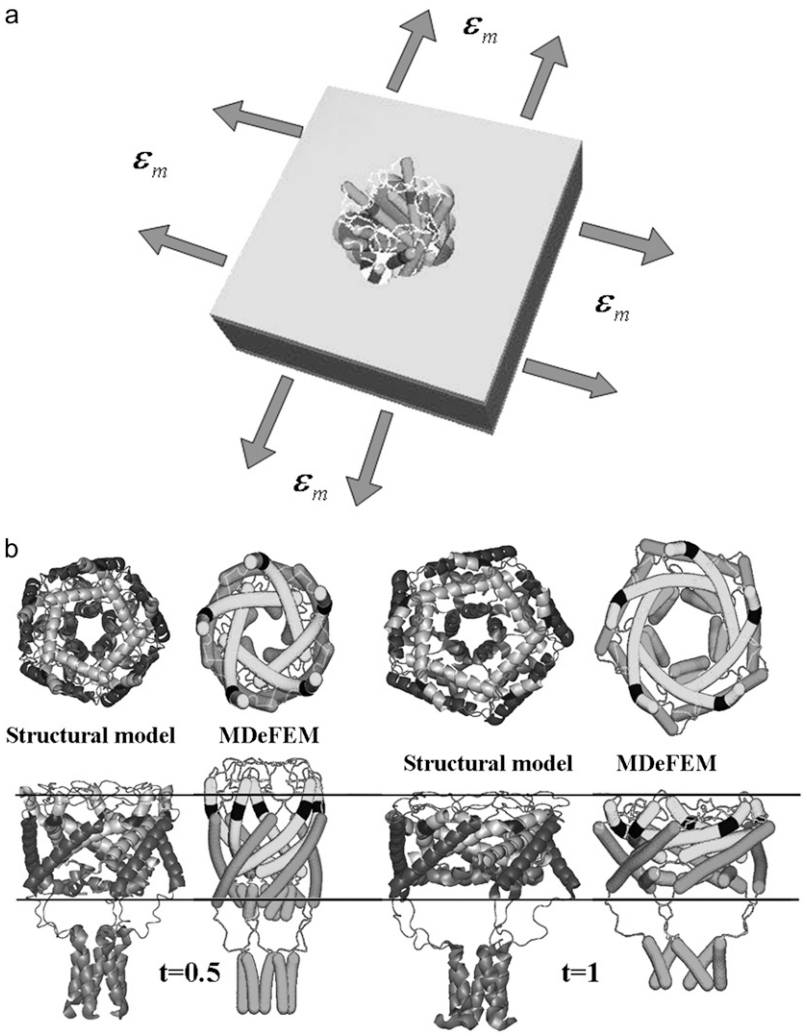

FIGURE 1 Equibiaxial tension. (*a*) Schematic of the MDeFEM continuum model. (*b*) Gating pathways of *E. coli*-MscL at half- and fully opened states: comparisons between the structural model (6) and the refined MDeFEM simulation (maximum membrane strain 21%).

The evolution of the pore radius obtained from MDeFEM simulation is comparable to that in the all-atom molecular dynamics (MD) study (5). The maximum membrane strain in steered MD (SMD) (5) is estimated to be ~5.4% (9) and we assume its increment is proportional to the time step used in SMD. As shown in Fig. 2 *a*, although the channel was far from fully opened in the nanosecond steered MD simulation, the relationship between the pore radius increment and membrane strain in the SMD (*open-square curve*) is in good agreement with the MDeFEM model at small strain, which nicely demonstrates that the continuum model has a reasonable description for the forces involved in the gating process, yet is capable of overcoming the length- and timescale limits to achieve a much larger pore-opening.

Despite the apparent success of the MDeFEM approach, the monotonic behavior found for the pore radius in Fig. 2 *a* suggests that the effective energy surface is essentially downhill toward the open state in the presence of tension. This is inconsistent with the energy profile estimated in Sukharev et al. (10), which involves the closed, intermediate, and opened states separated by sizable barriers, even in the presence of tension; in addition, the radius of the channel in the opened state is well defined and is essentially unchanged in a wide range of tensions in experiments. To capture the realistic behavior of the channel with such an energy landscape, further refinement of the continuum mechanics model is needed, especially the treatment of solvation, because it has been proposed (3,11,12) that solvation stabilizes the open state of MscL in which hydrophilic residues become exposed to solution (see more discussions later in the section ''Limitations of the current implementation'').

The variation of the averaged tilting angle of TM1 helices, measured from the principal axes of TM1 helices and averaged over the five subunits, is given in Fig. 2 *b* as a function of the MscL radius increment ratio (*solid-circle curve*). The decrease of the tilting angle is almost monotonic with the increase of membrane strain, and the MDeFEM simulation result agrees qualitatively with that of the structural model in the half- and fully opened states (6).

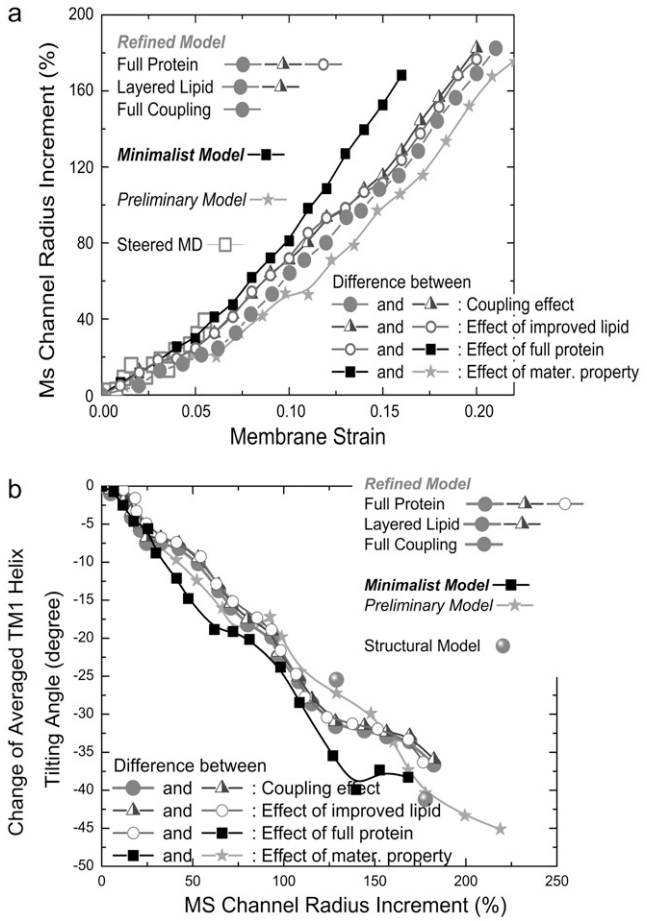

FIGURE 2 Upon equibiaxial tension and comparison of different levels of model sophistication (see text), (*a*) the evolution of the effective pore radius of *E. coli*-MscL versus membrane strain, and (*b*) the change of TM1 helix tilting angle versus the effective MS channel radius.

Comparison of continuum models of different sophistication

As discussed in the section ''Elements of the MDeFEM framework'' of Part I, the MDeFEM model presented in this work has greatly expanded beyond that in the preliminary study (9), and the main differences are: i), inclusion of all essential protein components including loops and cytoplasmic helices, rather than only the transmembrane helices; ii), adoption of a more realistic three-layer model for the membrane versus the homogeneous elastic sheet; iii), including the concurrent coupling between lipid and protein deformation instead of only the one-way coupling in the preliminary study (9); and iv), refinement of elastic and interaction parameters of the continuum components based on additional atomistic simulations instead of simply adopting literature values. In this subsection, we analyze the effects of these improvements by removing their contributions one item at a time. Although there is still plenty room for improvement, we refer to the most complete model in this work (see Fig. 1 *a*) as the ''refined'' model in subsequent discussions.

Starting from the refined model (*solid-circle curve* for the pore evolution in Fig. 2 *a*), we first remove the concurrent coupling by carrying out a two-stage simulation similar to the previous study (9) (the subsection ''Current status of numerical simulation of MscL and their limitations'' in Part I), which assumes that the configuration of protein is completely dictated by the membrane deformation. The results are given as the triangle curve and its difference from the solid-circle curve is the effect of coupling; as shown in Fig. 2 *a*, the effect is only ~5% (the concurrent coupling makes gating slightly more difficult). We note that such estimation may be overly optimistic, because if the lipid model is made more liquid-like rather than a solid (see the section ''Limitations of the current implementation''), the protein deformation should have more impact on membrane strain and thus the concurrent coupling would become more important.

As the next simplification, we replace the three-layer lipid model by the homogeneous model with equivalent elastic properties derived in the ''In-plane tension'' section in Part I, and the results are given as the open-circle curve in Fig. 2 *a*. By comparing with the triangle curve, it is seen that the effect of different lipid models is also rather small in terms of affecting the evolution of the MscL pore radius, primarily because the fitted Poisson's ratio is the same for the headgroup and tail layers in the three-layer lipid model for palmitoyloleoylphosphatidylethanolamine (POPE). It is important to remark that this appears to be an artifact of the current continuum model because MscL gating is known to be sensitive to lipid pressure profile (or composition) (13). On the other hand, if a different lipid bilayer is chosen and there is a mismatch between the effective Poisson's ratios of the headgroup and tail layers in the continuum model, we expect to observe more significant differences between the three-layer and homogeneous lipid models.

Next, the model is further simplified by replacing the protein with a ''minimalist model'' that includes only the transmembrane portion, similar to that in the preliminary study (9) (see Fig. 4 *b* in Part I although an *E. coli*-MscL is studied in this article); the only difference is that the material properties of the TM1/TM2 helices and lipid are those summarized in Table 1 of Part I rather than those obtained from literature in the preliminary study (9). The comparison between the solid-square curve and the open-circle curve in Fig. 2 *a* shows the effect of simplifying the protein model, which demonstrates that the incorporation of cytoplasmic helices and loops make it more difficult for the channel to open, although the magnitude of the effect is modest.

Finally, comparing the preliminary result in the preliminary study (9) (*solid-star curve* in Fig. 2 *a*) and the minimalist model (*solid-square curve*) yields the effect of the refined material parameters. As expected, in the case where membrane deformation has the dominant effect and the MS channel radius is governed by the deformed helices, the moduli of continuum components play a major role, and the gating pathway should be system-dependent.

With material properties specified for the *E. coli*-MscL, comparing the preliminary and the more elaborate (refined) model in this work (*black-solid-square curve* versus *solid-circle curve*), the pore radius evolution in Fig. 2 *a* shows that the minimalist model is only ~20–25% different, in part due to error cancellation. Likewise, the changes in the average tilting angles of TM1 helices during gating are very similar (Fig. 2 *b*) with different levels of sophistication (or refinement), all showing a rather monotonic behavior. Therefore, the gating characteristics of MscL are largely dictated by the lipid deformation and the transmembrane segments are the most critical components of the channel in this regard. This finding underpins the development of analytical models (the ''Analytical models'' section of Part I), whose performance will be compared with the refined and minimalist models below.

Effect of structural motifs

To investigate the functions of different structural components of protein during the gating transition, which is an important goal for biophysical studies of MscL in general (6,8), individual groups of structural motifs are systematically removed and the effects on gating are analyzed. As a reference, the conformation of the *E. coli*-MscL in the fully opened state is given in the left column of Fig. 3, which is obtained with the maximum membrane strain of 21%.

First, the loops connecting TM1 and TM2 helices are removed and the new structural configuration at 21% membrane strain is given in the second column of Fig. 3. Compared with the full protein model, the absence of the TM1/TM2 loop reduces the averaged TM1 tilting angle by ~10°. In other words, the presence of these loops limits the opening of the top part of the transmembrane pore. In addition, without the coordination of the relatively stiff loops, the bending of TM1 and TM2 helices becomes more prominent. Due to the increased curvature of deformed TM2 helices, the shape of the S3 bundle is affected (although it still remains almost closed); likewise, the pore enclosed by S1 helices is enlarged slightly due to the different changes in TM1 helices. The channel radius (enclosed by TM1 helices), however, is not significantly perturbed (a quantitative measurement is given below). Thus, these results suggest that the loops connecting TM1 and TM2 helices are moderately important.

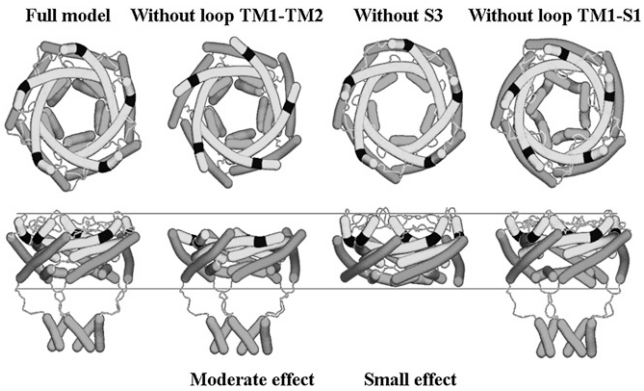

FIGURE 3 Effects of protein structural motifs: the conformational configurations of *E. coli*-MscL at equibiaxial membrane strain of 21%.

Next, we remove the S3 helices and also the loops connecting the S3 and TM2 helices; the results are given in the third column of Fig. 3. Because the S3 bundle is ''isolated'' in the cytoplasmic region from the main protein complex, its removal does not have any major impact on the deformation in transmembrane region: both pores enclosed by the TM1 bundle and the S1 bundle are essentially unchanged. The TM2 bundle shape is affected due to the removal of its ''tie'' to S3, although the effect is very small.

Finally, all structural components are kept except the loops that connect TM1 and S1 helices. As seen in the fourth column of Fig. 3, without the ''guidance'' of these linkers, the S1 pore becomes distorted in the transmembrane region and hence both the TM1 and TM2 helices are affected. This illustrates the importance of the loops between the TM1 and S1 helices.

At a more quantitative level, as shown in Fig. 4, the evolutions of pore radius and the TM1 helix tilting angle are not sensitive to the removal of the S3 bundle, whereas removal of the loops (either the TM1/TM2 or S1/TM1 linker) leads to a wider pore in the open state. In other words, the loops slightly constrain gating.

Most of these findings are in qualitative agreement with features of the structural model constructed based on experiment constraints (8), which suggest that the loops connecting the TM1/TM2 helix bundles and those connecting the TM1/S1 helix bundles play important roles in the gating process whereas the S3 helix bundle remains essentially static during gating.

Comparison with analytical models and elastic network models

Effective continuum medium model (ECMM)

From the derivation in the subsection ''Closed form solution for *E. coli*-MscL'' of Part I, the lower and upper bounds of the pore radius increments upon equibiaxial deformation, $\Delta a_{\mathrm{ECMM}} = 0.98\Delta c$ and $\Delta a_{\mathrm{ECMM}} = 0.31\Delta c$, respectively, are proportional to the lipid cavity radius expansion Δc, which is in turn related with the membrane strain ε_{m} as $\Delta c = 2c\varepsilon_{\mathrm{m}}/(1-\bar{\nu})$. In Fig. 5, the upper and lower bounds Δa_{ECMM} versus ε_{m} are given as straight lines. They bound the pore radius evolution curves of the refined and minimalist models quite nicely, despite of the simplicity of ECMM.

Elastic network model (ENM)

The ENM can reveal more structural details than ECMM through simplified analytical formulations of atom interactions. Results from various ENM-based pulling simulations (the

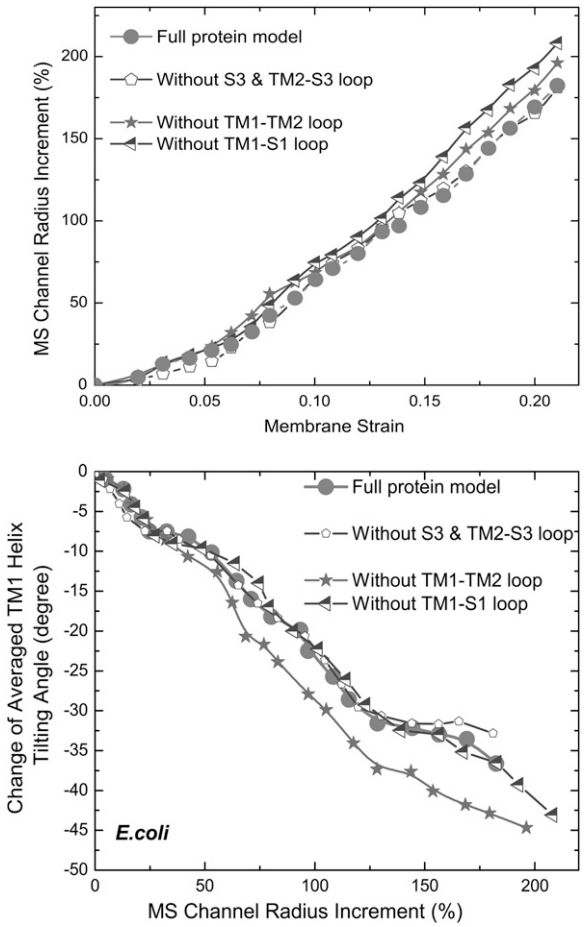

FIGURE 4 Effects of protein structural motifs: the increment of effective pore radius as the membrane strain is varied.

protocols are summarized in Table 3 in Paper I) are presented in Figs. 6–8. We focus on equibiaxial tension, the most effective loading mode for gating (see below), although ENM can be readily extended to other loading modes. During each simulation, the displacement boundary conditions used for pulling selected atoms are related with the far-field equibiaxial membrane strain, based on the derivation in the ''In-plane tension'' section in Part I. To accommodate large deformations, the simulation is divided into several ($\sim$10) steps, and after each step, the Hessian matrix of the entire system is recomputed with respect to the updated configuration.

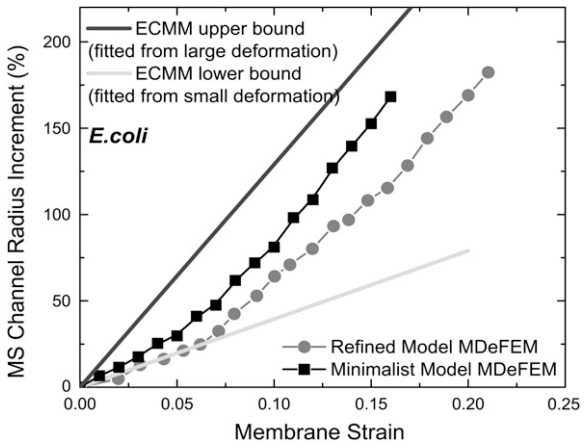

FIGURE 5 ECMM compared with the refined and minimalist models (upon equibiaxial tension).

The key geometrical properties that characterize the gating transition include the expansion of the effective pore radius (Fig. 6 *a*) and the change of angles of the TM1/TM2 helices (Fig. 6, *b* and *c*) during the simulation. Despite that the united all-atom ENM includes side chains, the effective pore radius is measured using the projection of the principal axis of TM1 helices (Fig. 6 *a*), and the tilting angle of the helices is measured based on the principal axis of the TM1 helix and averaged over the five subunits (Fig. 6 *b*); both measurement methodologies are consistent with those presented earlier. In the inset of Fig. 6 *b* and also in Fig. 6 *c*, the inclination angles are measured differently and are based on the top and bottom ends of the helix and averaged over the subunits; since the end atoms may change during the simulation; this particular measurement leads to a smoother variation (compare with that in Fig. 6 *b*). Among the ENM-based pulling protocols, these properties evolve in a similar fashion except with Protocol 1-3, in which only part of TM2 is explicitly pulled. In this set of simulations, the pore remains substantially more closed than that predicted by other pulling simulations because the TM1 helices only move slightly; correspondingly, the tilting angles of the TM1 helices (Fig. 6 *b*) change more slowly compared with other pulling simulations, although the TM2 helices tilt at a similar pace. These observations clearly illustrate that TM1 helices need to respond actively to tensions in the lipid (mimicked by either direct pulling or through explicit membrane-TM1 interactions in other ENM simulation protocols) rather than simply following passively the TM2 helices for a successful gating transition; in other words, the exposure of TM1 to the lipid membrane is critical for gating. For the rest of the pulling simulations, the evolutions of the effective pore radius and tilting of TM1/TM2 helices are largely similar.

The qualitative trends are also consistent with the findings from the MDeFEM simulations, where the corresponding curves from the minimalist and refined models are given in Fig. 6. For example, the tilting angle of the TM1 helices from the structural model (6) is $-41°$ for the open configuration (see Fig. 2 *b*), and the corresponding values from the MDeFEM and most pulling simulations (except Protocol 1-3) are $\sim -37°$ and $-43°$, respectively (see *main panel* of Fig. 6 *b*). The pore radius increment found in ENM is rather smooth and almost linear, which indicates that the deviation of the ENM model from linearity due to changes in the Hessian matrix during the pulling simulations is relatively small.

The inclusion of all heavy atoms (both main-chain and side-chain atoms) in the ENM makes it possible and worthwhile to compare the predicted open conformation and the

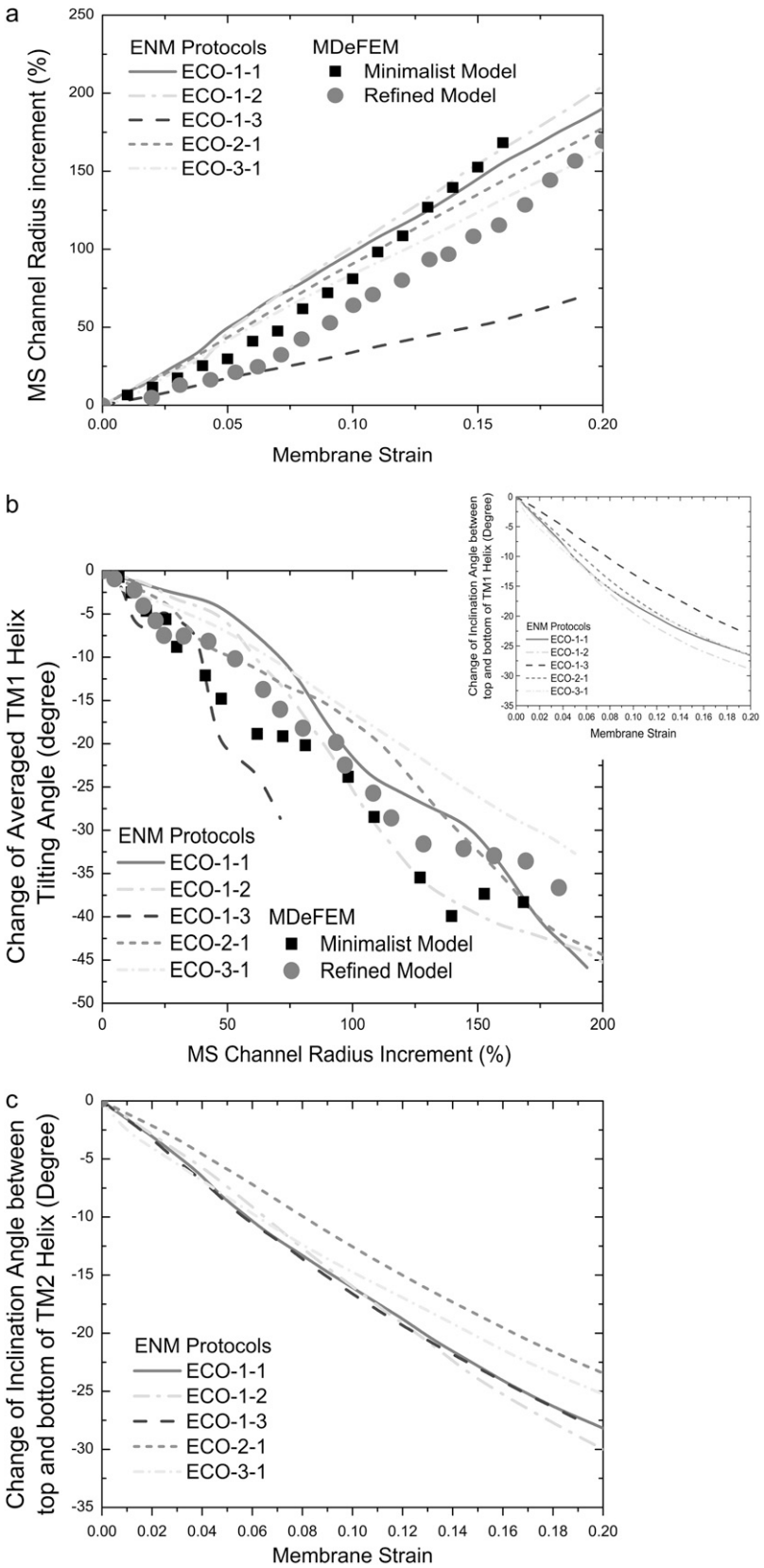

FIGURE 6 Structural properties of the *E. coli*-MscL during various pulling simulations based on the elastic ENM. The pulling protocols are summarized in Table 3 of Part I; in Protocols 1-1, 1-2, and 1-3, selected backbone atoms are pulled explicitly in a radially outward fashion, in Protocols 2-1 and 3-1, an elastic membrane bilayer is included explicitly and the outer layer of lipid atoms is pulled in a radially outward fashion. (*a*) The increase of the effective pore radius, (*b*) the change in the average tilting angles of TM1 helices, and (*c*) the change in the average inclination angles of TM2 helices during the ENM simulations, as the corresponding equibiaxial membrane strain is varied. The results from MDeFEM are also shown. In the main panel of *b*, the tilting angles are measured from the principal axes of TM1 helices and averaged over the five subunits. In the inset of *b* and also in *c*, the inclination angles are measured using the top and bottom atoms of helices and then averaged.

structural model of Sukharev and Anishkin (6). In fact, the incorporation of more structural details, such as side chains, is an advantage of ENM over MDeFEM. The predicted open ENM structures are superimposed with the open structural model in Fig. 7, which shows good qualitative agreement.

In addition, we examine the pore-size profile along the z axis of MscL in the predicted open conformation using the HOLE program, which computes the size of the largest sphere that can be inserted at a given z level (based on the backbone atoms); note that the pore size referred to in this subsection is smaller than the effective pore radius used elsewhere. As references, the profiles for the closed and open states according to the structural model (6) are also compared with ENM results in Fig. 8.

There are several interesting trends in the pore-size profiles (Fig. 8). First, the pore size is significantly smaller with Protocol 1-3 around $z \sim 0$ Å, which is close to the base of TM1

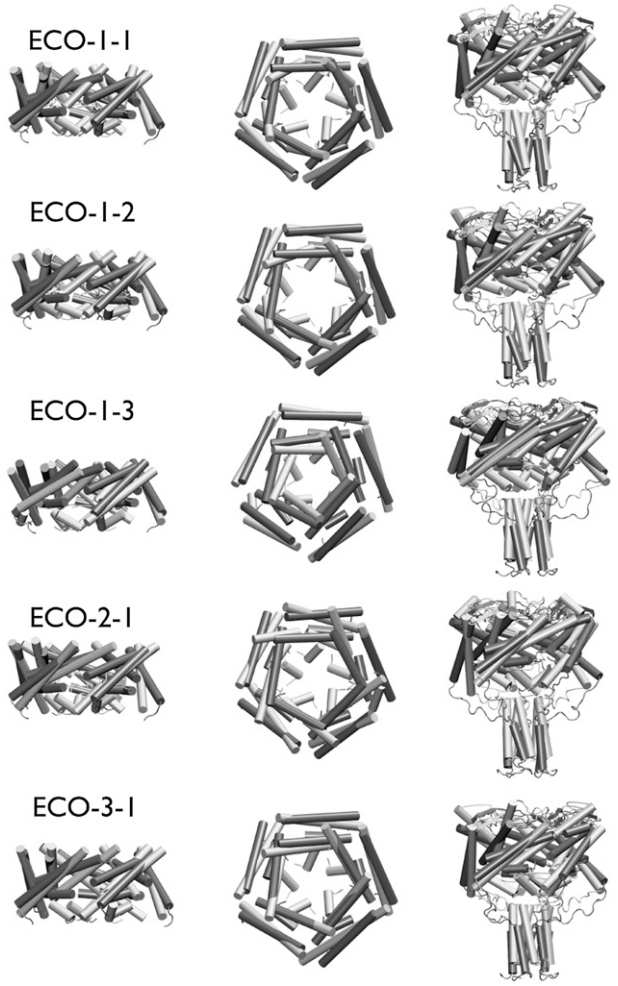

FIGURE 7 Superposition of the open-state structure in various ENM-based pulling simulations (*light*) with the open-state in the structural model (*dark*) (6). In addition to the relatively minor differences in the TM1/TM2 orientations, note the differences in S1 helices among different simulations and between simulations and the structural model (6) (see discussions in the text).

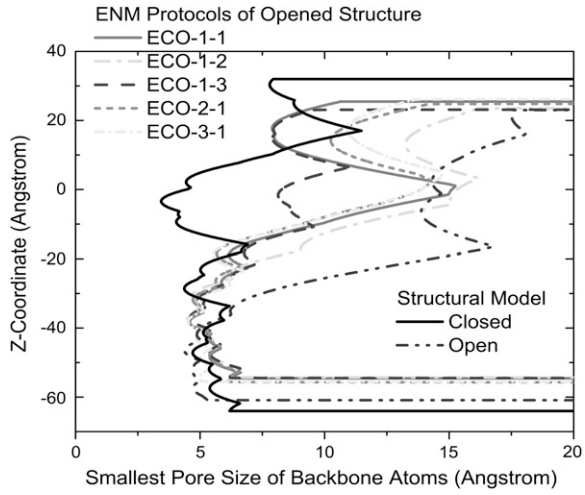

FIGURE 8 Pore-size profile for the predicted open-state ENM structure (with a corresponding membrane strain of ~20%) in various ENM simulations along the z axis (membrane norm) of the *E. coli*-MscL; $z = 0.0$ Å is at the membrane center. For reference, the profiles for the open and closed states in the structural model (6) are also included. The pore size is determined using the HOLE program while considering only the backbone atoms of the protein (and different than the effective pore radius referred to elsewhere in this article).

helices; this is because the TM1 helices are not explicitly pulled in Protocol 1-3 and therefore have substantially underestimated movements. Another region that shows significant differences among different pulling simulations centers around $z \sim 15$ Å, which largely involves the top of the TM1/TM2 helices and the periplasmic loops. In Protocol 1-1 and 1-3, these regions are not explicitly pulled and therefore they have only very limited displacements, which correlates to a narrow pore in the corresponding region. In Protocol 1-2, in which all backbone atoms within $|z| < 20$ Å are pulled explicitly, including the top of TM1 and TM2 helices (the backbone of TM1 spans z in the range of -13 to 16 Å; backbone of TM2 spans z in the range of -21 to 15 Å) as well as the periplasmic loops. As a result, the pore size around $z \sim 18$ Å is significantly expanded and in fact similar to that in the open model of Sukharev and Anishkin (6). In the protocols that include an explicit membrane, the close contacts between the membrane and the protein atoms near the $z \sim 18$ Å region lead to notable displacements in the protein as the membrane is stretched. Consequently, the pore size in this region is between the two limits observed above (Fig. 8). This observation once again highlights the importance of protein-membrane interaction, not only for the transmembrane helices but also periplasmic regions close to the membrane. We note that a recent MD simulation (14) also emphasized the importance of interactions between the lipid and residues in the top section of the transmembrane helices for stabilizing the open conformation.

Concerning other structural motifs, the S3 helices have very minor structural changes, similar to the observation in the MDeFEM simulations. Moreover, it is interesting to note that the S1 helices remain largely intact in all the ENM

simulations. The only slight exception is in Protocol 1-2 where part of S1 is under explicit pulling due to the selection criterion of $|z| < 20$ Å (backbone of S1 spans z between -30 and -17 Å); as shown in both Figs. 7 *b* and 8, the pore enclosed by the S1 helix bundle is slightly expanded compared to the predictions from all other pulling simulations. Nevertheless, the magnitude of the structural response in S1 is much smaller compared to that proposed in the structural models (6), in which the S1 helix bundle completely disassembles in the open state (Figs. 1 *b* and 7); we note that MDeFEM predicts a moderate expansion of the S1 helix bundle, although the opening of the S1 pore is less dramatic than that in the structural model (the ''Conformational transition'' subsection and Fig. 1 *b*), and whether the situation holds upon improving (hydrophobic) interactions among helices in the MDeFEM model remains an interesting point. As noted by Sukharev et al. (6,8,15), such a dramatic conformational change in the structural model is consistent with the experimental data that support the idea that the S1 helix bundle forms the second gate for MscL. We note, however, that there may be an uncertainty in the precise conformation of the S1 segment in *E. coli*-MscL. For example, the N-terminus is disordered in the original x-ray structure of the *Tb*-MscL; in a more recently refined model, the N-terminus is better fitted, but they point outwards to the protein-membrane interface instead of forming the helical bundle assumed in the structural model. It is not clear if the orientation in the new x-ray model is consistent with the cross-linking data that suggested close proximity of S1 helices in the closed state, but the cross-linking experiment was done in *E. coli*. Finally, the presence of the His tags in the proteins used for x-ray studies may also perturb the conformation of the N-terminus. In other words, there are ambiguities in the orientation of the S1 helices of *E. coli*-MscL that might be the origin for their different structural responses in our ENM pulling simulations and the structural models of Sukharev et al. (6) In fact, using the new x-ray model for *Tb*-MscL in conjunction with Protocol 2-1, we also observed expansion of the S1 segments since most of S1 are in contact with the membrane (data not included). Clearly, it remains an interesting task to determine the conformation of the S1 segments in MscL, especially for both the closed and open states of *E. coli*-MscL.

DEFORMATION UNDER OTHER IN-PLANE DEFORMATION MODES

Besides the most relevant equibiaxial tension mode discussed extensively in the previous section, uniaxial tension and shear are two other basic in-plane deformation modes for the membrane from a solid mechanics point of view, although they probably are less biologically relevant, especially when considering that real cell membranes are likely in the liquid crystalline phase rather than a solid. (On the other hand, considering that the cell membranes are complex structures that contain many components such as cholesterol and transmembrane proteins, they might be less fluidic than a pure lipid bilayer.) The study on these two modes, as well as those on other loads in the following sections, is aimed to explore whether MscL is unusually sensitive to specific mechanical stimuli and essentially inactive to others, from a pure ''solid'' point of view.

Upon uniaxial tension, since the lipid cavity is stretched along the tension direction while it shrinks laterally, the MS channel also undergoes highly asymmetrical structural distortions. The distortion is more dramatic in the case of pure shear. Fig. 9 compares the pore radius evolutions with increasing strain for the three in-plane modes. The effective pore radius is obtained from the refined model (unless otherwise denoted in the following sections). The pore area remains essentially unchanged during uniaxial loading whereas it decreases during shear; thus, both modes are far less efficient for stimulating opening of MscL, and equibiaxial tension is the most important perturbation to achieve full gating.

OTHER REPRESENTATIVE BASIC DEFORMATION MODES

As illustrated in Fig. 3 of Part I, the general load acting on a membrane can be decomposed into several basic deformation modes. The basic in-plane modes are investigated in the two prior sections above; other basic modes, which are often considered more complex and beyond the ability of typical all-atom simulations, are studied in this section. Simulating the response of MscL to these modes illustrates the value of the MDeFEM approach.

Bending

Membrane bending is another important mode for a flexible cellular structure, and becomes prominent during cell adhesion/contact. A four-point bend flexure of a circular membrane similar to that in our preliminary study (9) is used. A uniform

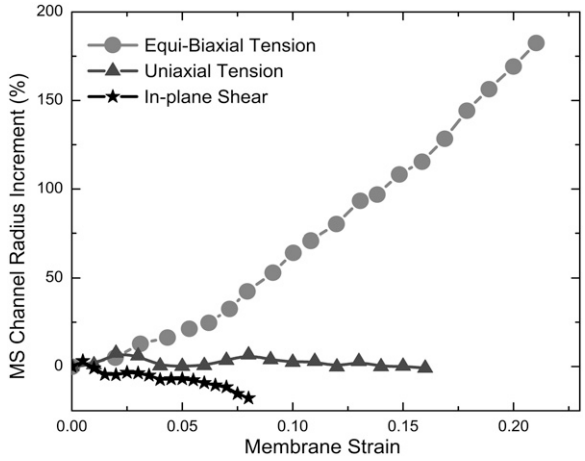

FIGURE 9 Effective pore radius increment as a function of membrane strain, under equibiaxial, uniaxial, and in-plane shear situations.

line load is applied at the outer boundary, which induces a distributed moment of 14.6 pN (the subsection ''Axisymmetric pure bending'' in Part I). The undeformed configuration of *E. coli*-MscL is given in the left of Fig. 10 where β is the ''cone angle''; before perturbation $\beta \sim 10^\circ$ and at the maximum bending moment β approaches zero.

During the axisymmetric pure bending, the wall of the lipid cavity rotates; however, its averaged radius throughout thickness remains about the same. Therefore, although the TM1/TM2/S1 helices become more upright, the transmembrane pore radius is only moderately increased. The S3 helices remain ''isolated'' and almost unperturbed. The snapshots at $t = 0.5$ and 1.0 are shown in the middle and right of Fig. 10, where the rotation and bending of the TM1/TM2/S1 helices are obvious. Finally, the TM1 bundle becomes almost upright within the transmembrane region.

At a more quantitative level, variations of the effective pore radius and TM1 helix cone angle are given in Fig. 11, *a* and *b*, respectively. We compare both the refined MDeFEM model and minimalist model. With increasing bending curvature, the pore radius first increases to ~6%, then decreases to ~−8%, and finally the pore radius increases to ~12% at the maximum bending moment. Such oscillation is due in part to the tilting of the TM1 bundle (which increases the pore radius) and due also to the sliding of TM1 helices (which decreases the pore radius); this feature is found in both the refined MDeFEM model and the minimalist model, although details are slightly different due to the constraints of various loops and cytoplasmic helices in the refined model. Overall, it is clear that axisymmetric pure bending does not lead to an obvious opening of the channel, and the curvature effect is important only when it's superimposed with membrane tension strain (e.g., due to excessive bending) (13,14,16).

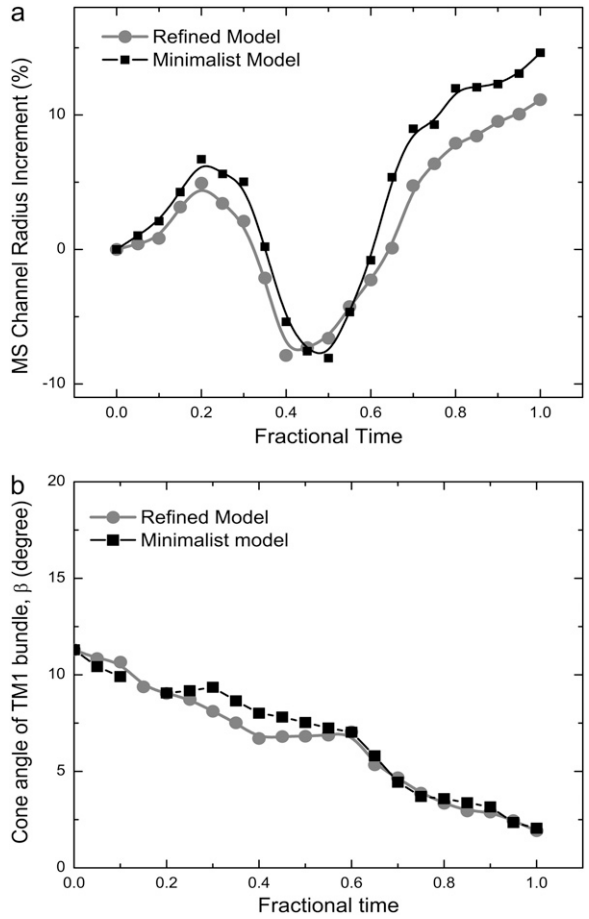

FIGURE 11 Axisymmetric pure bending and comparison between refined and minimalist models: (*a*) increment of the effective pore radius and (*b*) change of the TM1 helix bundle cone angle β.

Torsion

Torsion in the membrane may occur if a cell is adhered to a substrate and then rotates; this clearly relies on a solid-like description of the membrane. We simulate clockwise and counterclockwise torsions of a solid-state membrane containing MscL. Since the lipid cavity radius is essentially unchanged during torsion, the effective channel radius oscillates (Fig. 12) with the torsion angle due to the many body interactions similar to those involved in bending. The final pore radius is actually smaller than the undeformed size, for torsions in both directions. This result shows that like pure bending, torsion (even if it can occur in the realistic cellular context) is not an effective mode for inducing the opening of MscL.

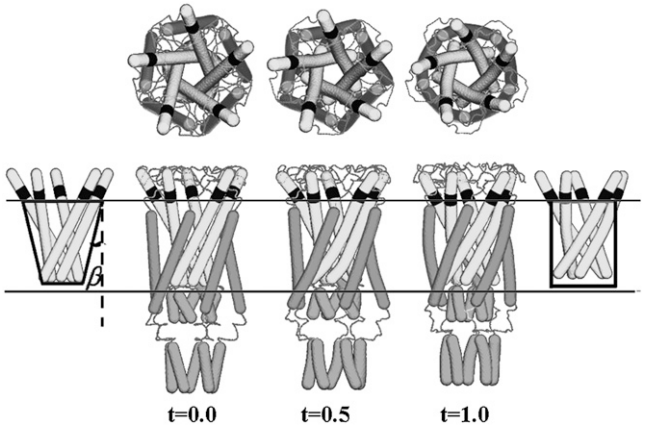

FIGURE 10 Gating pathways of *E. coli*-MscL when the membrane is bent upward.

INTERACTION BETWEEN TWO MscL MOLECULES

Since the gating transition of MS channels relies on deformation of the membrane, it is reasonable to expect that MS channels in close proximity may significantly influence each other's gating behavior. This is a particularly interesting issue, considering the fact that a biological membrane is highly heterogeneous and rich in proteins and other biomolecules

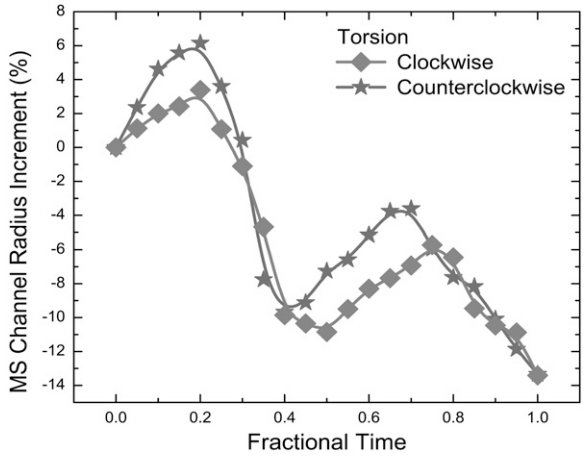

FIGURE 12 Effective MS channel radius increment under torsion.

such as polysaccharides. In this work, we limit our attention to the most important loading mode, equibiaxial tension; the goal is to explore the configuration of *E. coli*-MscL as the center-to-center distance of the protein, λ, is varied. The snapshots of the top view and bottom view of the channel, at the same maximum membrane strain of 21%, are given in Fig. 13.

When the two proteins are separated far apart, $\lambda > 200$ Å, they do not sense the existence of the other and thus the conformation (*first column* in Fig. 13) is exactly the same as that of an isolated channel (Fig. 1 *b*). With the decrease of separation, at $\lambda = 90$ Å, Fig. 13 shows that the TM1 pore becomes distorted and the two channels start to affect each other. With a continued decrease of inter-MscL distance, $\lambda =$ 70 Å and $\lambda = 60$ Å, the distortion of pore is more visible; the pore becomes more elliptical and the pore radius decreases slightly. The tilting angle of the transmembrane helix is not affected much. Thus, two *E. coli*-MscLs start to significantly influence each other when their center-to-center distance is smaller than ~100 Å.

To quantify the critical separation below which the MscLs start to interact strongly, in Fig. 14 we plot the bias ratio (between the short and long axes of the TM1 pore at maximum

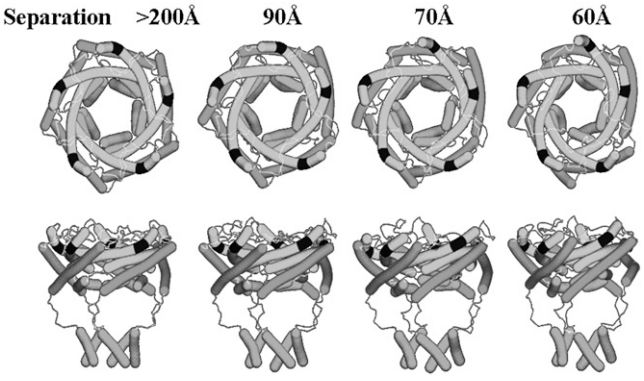

FIGURE 13 Interactions between two *E. coli*-MscLs: at an equibiaxial strain of 21%, the structural configurations of *E. coli*-MscL with the center-to-center separation $\lambda = 200$, 90, 70, and 60 Å.

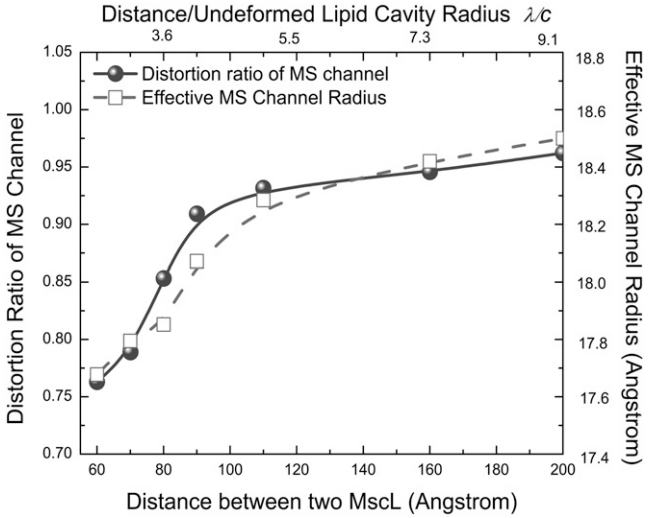

FIGURE 14 Cooperativity between two *E. coli*-MscLs: (*a*) the bias ratio versus channel separation and (*b*) the effective radius of the channel versus channel separation.

membrane strain) of the pore as a function of λ. In the axis on top of Fig. 14, the separation is normalized by the undeformed lipid hole radius, c. When the two channels are far apart, the bias ratio is 1. The bias ratio decreases gradually with the reduction of λ; when λ/c falls below ~4, the reduction of the bias ratio is accelerated, which means that the two channels start to interact more intensively. Fig. 14 also gives the variation of the effective channel radius (at $\varepsilon_m = 21\%$) versus λ and λ/c. Again, the reduction of pore radius is moderate until λ/c is smaller than ~4. Thus, Fig. 14 reveals that the critical separation is ~100 Å, which is close to four times the radius of the undeformed lipid cavity. This finding is qualitatively consistent with the prediction based on the classic plane stress solution (the ''Protein interaction'' subsection in Part I).

In a recent theoretical study (17), Ursell et al. also analyzed the cooperativity between two MscLs using a different continuum mechanics model for the membrane-protein system. They also observed significant interaction between the two channels at distances below ~100 Å, similar to our work. However, it is worth emphasizing that our study and that of Ursell et al. (17) address different aspects of the channel-channel interaction. In this work, we study changes in the pore size due to the presence of another channel at specific membrane tension. In Fig. 14, the reduction of the MscL pore radius is entirely due to distortion in the pore shape, and such a feature is absent in the Ursell et al. study (17), where the proteins were treated as simple objects with cylindrical symmetry. (From solid mechanics theory (the ''Protein interaction'' subsection in Part I) it can be shown that with two circular holes present in a thin elastic sheet, the area of the pore is essentially unchanged when the sheet is stretched biaxially. Therefore, the small MscL pore radius reduction observed in Fig. 14 is entirely due to pore distortion.) In their work (17), where the thermodynamic model focuses on the treatment of

the lipid, especially near the channel-lipid interface, Ursell et al. studied the contribution from membrane deformation to the association of membrane proteins with similar signs of hydrophobic mismatch and change in the gating threshold. Their analysis revealed cooperative gating (i.e., lowering of the gating threshold), which was explained by the argument that the total membrane energy containing two ''open'' channels can be reduced when they are close to each other; once again, the protein deformation free energy and structural distortion were not considered. In other words, our continuum model, which attempts to describe contributions from both protein and lipid deformations in a balanced manner, is different from the lipid-centric framework pioneered by Phillips and co-workers (17). With further improvements in the MDeFEM model, especially concerning the treatment of membrane (such as incorporating local residual stress and membrane curvature near the protein (see below), the cooperative behavior of multiple channels in the membrane can be analyzed in a more quantitative fashion. More importantly, we note that our conclusion and the findings by Phillips and co-workers (17) are not necessarily contradictory to each other; i.e., it is possible that the gating threshold is lowered due to cooperativity whereas the current through each channel is smaller due to distortions in the pore shape. These trends can be tested by careful channel recording studies.

SIMULATION OF LABORATORY EXPERIMENTS

Although the MDeFEM approach has been validated by both structural model (6) and steered MD simulation (5), it is still desirable to directly compare its performance to experiments. In addition, simulating the complex, large-scale deformation of lipid vesicle in experiment would further demonstrate the power and efficiency of MDeFEM. Indeed, interesting variations are found in the structural response of MscL in the current ''numerical experiments'', which we hope will stimulate new experimental studies for verification.

Specifically, we explicitly simulate the structural response of *E .coli*-MscL to realistic mechanical loading patterns found in two common types of experiments. First, we simulate the patch clamp experiment on a lipid vesicle, which is widely used in channel studies (4). Second, we simulate a hypothetical indentation experiment on the same liposome. Nanoindentation is an alternative experimental technique to explore the mechanical behaviors of small organisms and material structures (18). Charras and Horton (19) used an atomic force microscopy tip to explore stretch-activated ion channels due to contact and the relevant stress. The model for experiment is kept simple to illustrate some essential aspects of the MDeFEM framework, which can be further improved to best mimic the experimental conditions.

The patch clamp experiment

The patch clamp experiment is sketched in Fig. 15 *a* for the undeformed and deformed configurations. The idealized lipid vesicle is taken to be a spherical liquid-filled shell, assuming that the membrane is not permeable (7). The bulk modulus of cytoplasm is similar to that of pure water (2.2 GPa) when the liposome is under high pressure (20). The diameter of the vesicle is 5 μm, which is in the middle of the size range of the liposome used in patch clamp experiment (7).

For simplicity, we take the problem to be axisymmetric by keeping the pipette normal to the substrate. The wall of the rigid pipette has a thickness of 0.2 μm and an inclination angle of 10°; the opening of the pipette is 1 μm (10). The contact between the liposome and the pipette is assumed to be frictionless. In the undeformed situation, the bottom surface of pipette just touches the vesicle. Next, suction pressure is applied on the portion of liposome membrane within the pipette pore to gradually bulge the part of membrane upward (*right configuration* in Fig. 15 *a*); with

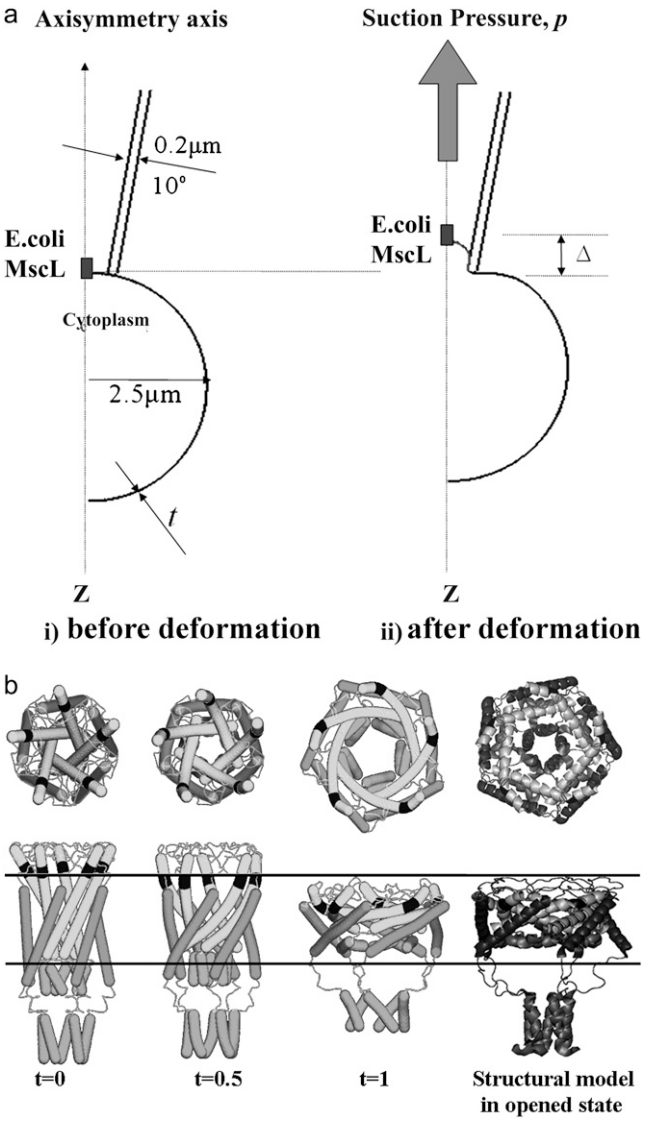

FIGURE 15 Patch clamp experiment: (*a*) schematic of the experiment and location of MscL and (*b*) the gating pathways of the *E. coli*-MscL.

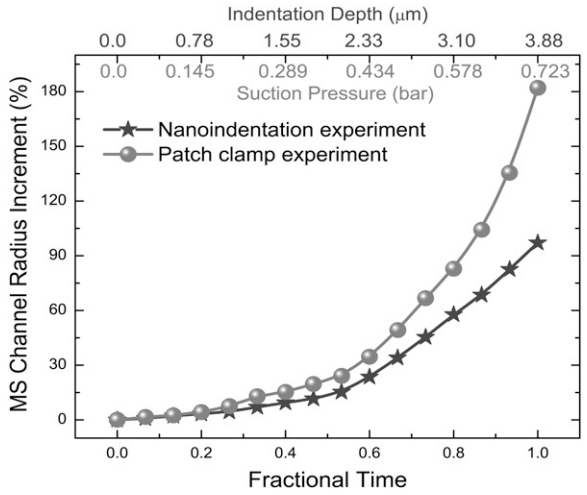

FIGURE 16 Simulation of lab experiments: the channel radius increment versus suction pressure in patch clamp experiment and indentation depth in indentation experiment.

the increase of suction pressure, p, the area of the membrane cap sucked into the pipette also increases and the force boundary condition is continuously updated. We assume that the *E. coli*-MscL is located at the north pole of the vesicle during the experiment, thus the stress field around it is equibiaxial. The suction pressure is increased until the stress needed for full MscL gating is reached. We note that the curvature of deformed membrane is not important in this case, because the pipette opening size is much larger than that of the MscL.

With increasing suction pressure (up to ~0.7 bar), the local stress near the channel at the north pole increases nonlinearly. Since the vesicle radius and the opening of the pipette are much larger than the protein dimension, the curvature of the membrane sucked in by patch clamp has a negligible influence, and the results of gating pathways (Fig. 15 *b*) are very close to that upon equibiaxial tension on a flat membrane (presented in Fig. 1 *b*). The final opened state has a configuration that is close to the structural model (6).

In Fig. 16, the increment of effective pore radius is plotted as a function of the suction pressure as the solid-circle curve. Although the relationship between the pore radius increment and membrane strain is almost linear upon equibiaxial tension (Fig. 2 *a*), due to the nonlinear coupling between membrane stress and suction pressure, the pore radius varies nonlinearly with pressure in the simulated patch clamp experiment.

In the previous patch clamp experiment (10), the effective Young's modulus of the membrane was ~18 MPa (see the estimation in our preliminary study (9)—the effective modulus is likely to be underestimated, because the estimation was based on the bulge test formula that requires the nonslip boundary condition. Although our finite element method simulation shows negligible slip at the opening of the pipette, during the patch clamp experiment, the ''slippage'' of lipid monolayer arises, which could underestimate the lipid modulus); the maximum membrane tension was ~3.4 MPa (measured when the suction pressure was ~60 mmHg) and thus the membrane strain was ~13% when the gating probability was 50% (10). In our simulation, at a maximum suction pressure of 542 mmHg, the maximum strain is ~21% that corresponds to the fully opened state (100% gating probability)—thus if the area of pore is half of the fully opened state, the required membrane strain is ~14%. In terms of the area enclosed by the MS channel, the membrane strain at which gating may be measured via experiment agrees qualitatively between the simulation and patch clamp experiment. (If the lipid modulus used in the patch clamp experiment is underestimated, the membrane strain should be smaller than 13% and thus there is more discrepancy with numerical simulation.)

The nanoindentation experiment

The configurations of nanoindentation are sketched in Fig. 17 *a* for undeformed and deformed liposomes. A rigid spherical indenter with a diameter of 2 μm is applied to perform the experiment, and a rigid substrate supports the bottom of the vesicle during the test; all contacts among the membrane, indenter, and substrate surface are assumed to be frictionless. An indenter of similar dimension was used in a previous experiment on colloidosome (21), which can be readily obtained by melting and pulling the tip of a glass fiber. The initial position of the *E. coli*-MscL is assumed to be at the equator. The indenter moves downward by a prescribed displacement, and the maximum indentation depth is ~80% of the vesicle diameter (further increase of the load may lead to excessive local deformation that damage the membrane). Upon indentation, the deformed vesicle shape becomes pumpkin-like, with a concave surface in its center and a protruded (bulged) perimeter as shown in the second column of Fig. 17 *a*.

At the equator, the local stress field is not equibiaxial, and the hoop stress is about two times the longitudinal stress; both vary nonlinearly with indentation load/depth. Due to the different in-plane membrane stress components surrounding the MscL, the lipid cavity and therefore the TM1 pore deforms into a distorted elliptical shape (Fig. 17 *b*). The bias ratio between the short and long axes of the pore is ~0.70. Likewise, the gate enclosed by the five S1 helices is also asymmetrical, with a bias ratio of ~0.72.

Even at the indentation depth of ~80% of liposome diameter, due to the biased pore evolution, the area enclosed by the MS channel is still somewhat smaller than that required for full gating (*solid-star curve* in Fig. 16); this indicates that it is more difficult to achieve a fully opened channel via nanoindentation experiment or other mechanical perturbations of the similar pattern, compared to patch clamp.

We hope these calculations will stimulate nanoindentation experiments on liposomes, which should be feasible but to our knowledge have not yet been performed. It is envisioned

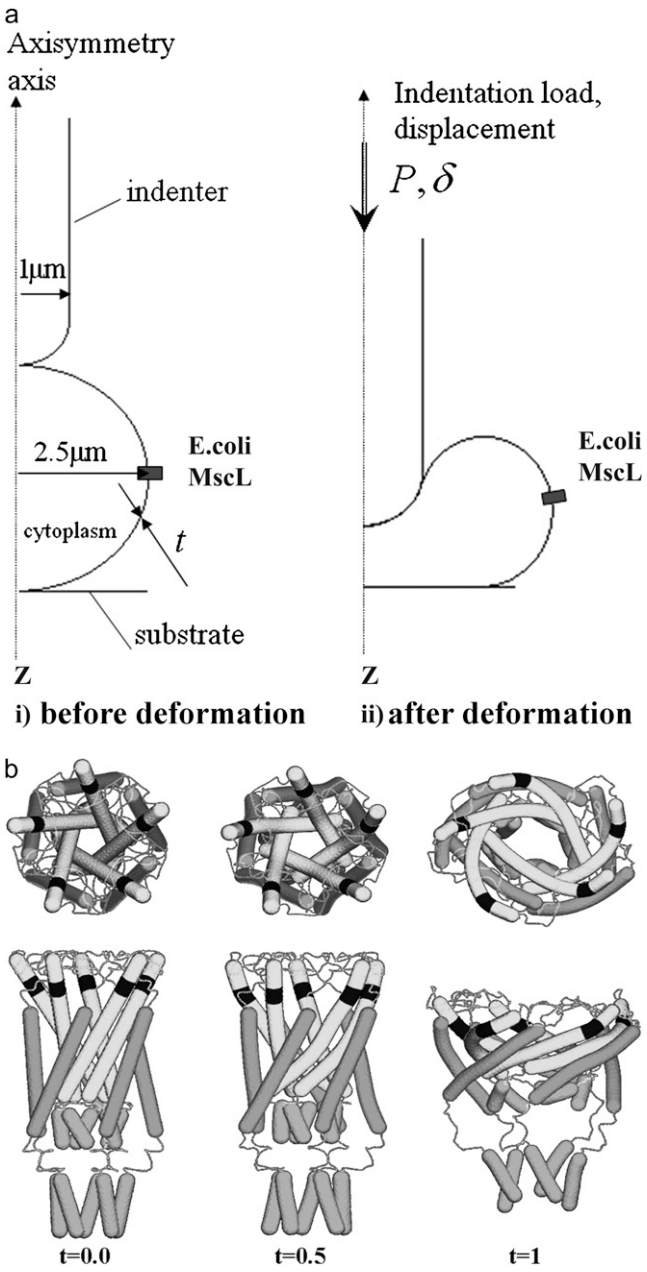

FIGURE 17 Indentation experiment: (*a*) schematic of the experiment and location of MscL and (*b*) the gating pathways of the *E. coli*-MscL.

that the flexible and versatile MDeFEM framework will enable numerical experiments with varying location, number, and properties of biomolecules/cells, as well as experimental conditions, and generate hypotheses that can be verified by experiments.

LIMITATIONS OF THE CURRENT IMPLEMENTATION

As discussed in Parts I and II, there are still many limitations in the current implementation of the continuum-based approach, and the model can be further improved with more realistic models and parameterization based on more elaborate atomistic simulations. For example, the helix mechanical properties can be assumed to be sequence-dependent and assigned with different tension, bending, and torsion stiffness in different regions. If this were done, helix kinking, which is known to play an important role in the gating transition of several channels (22), can be properly described. The mechanical properties can also be field variable-dependent, for example, varying with exposure to solvent. Nevertheless, the use of simple parameterization procedures in this study allows us to focus on the most fundamental physical principles that govern gating, and comparing our results to experiments points to features of the model that require more careful treatments.

Physically speaking, one of the major limitations in our study concerns the treatment of the lipid bilayer, which is taken to be an elastic solid slab whereas the realistic membrane should be more fluidic and cannot sustain large shear stress. This approximation, along with the lack of solvation contribution, leads to the exceedingly high membrane strain required for full gating, as discussed in the section, ''Gating mechanisms under equibiaxial tension''. Such artifact can be partially alleviated by introducing viscosity and anisotropy (especially the out-of-plane Poisson's ratio) to the lipid model. Through creep, anisotropic lateral deformation, and stress concentration, the lipid cavity surrounding MscL can be continuously enlarged and lead to channel opening at much lower tension stress (~10–15 dyne/cm) and membrane strain (around several percent); more detailed results of these new refinements will be reported elsewhere.

As repeatedly emphasized in discussions in earlier sections, the treatment of various interfaces in the system (protein/lipid, protein/water, and lipid/water) also deserves improvements. The lipid can be made more inhomogeneous by considering different properties at the headgroup/tail interface, as well as introducing local membrane curvature or residual stress at the channel/lipid interface to treat the distinct properties of annular lipids (23). In addition, it has been proposed that solvation plays an important role in stabilizing the open conformation of MscL due to the exposure of hydrophilic residues (3,11), and hydrophobic interactions among helices are expected to be an important driving force behind several key structural transitions, such as S1 undocking. The forces exerted by solvation can be superimposed to the mechanical forces during the gating process (L. Ma and Q. Cui, unpublished). Furthermore, the lateral interactions among continuum components, which complements the normal interactions considered in this article, should be included and they serve as ''drag'' or ''frictional'' forces to establish locally stable conformational states. Therefore, we expect that these improvements will eventually not only help reduce the membrane strain required for gating, but also lead to the proper free energy landscape sampled during the gating process, such as creating the pla-

teau of channel radius evolution during gating as observed experimentally.

CONCLUSION

The conformational transitions of a representative MS channel, the *E. coli*-MscL, are explored using the proposed MDeFEM approach when various loads are acted on the membrane: in-plane tension, bending, torsion, and interaction, as well as the more complex stress fields corresponding to patch clamp and nanoindentation experiments. Gating of MscL is intimately related with the mechanical properties of lipid and protein, which can be well represented by the continuum mechanics-based approach.

Equibiaxial tension is the most effective mode to achieve full channel gating. Gating is primarily realized by iris-like expansion of TM1/TM2 helices in the radial direction, as well as tilting of the subunits. The S1 and S2 helices move into the transmembrane region, and the S1 pore is also pulled open and becomes a part of the channel; the cytoplasmic S3 helices play a minor role in terms of mechanical functions. The loops connecting the TM1/TM2 and TM1/S1 helices are also important for regulating the gating of MscL. The transmembrane helices (TM1/TM2) are the most important protein components during gating, through the interaction with lipid membrane. The gating behavior is also system-dependent, i.e., strongly influenced by the details of geometry and properties of protein/lipid components. Even with a rather simple parameterization, the MDeFEM simulation for equibiaxial tension agrees reasonably well with the structural model, experiment, and all-atom (steered-MD) simulations. Considering the difficulty associated with accessing the fully open state of MscL in all-atom simulations even in the presence of a strong steering force, reproducing many experimental observations with the MDeFEM simulations is not a trivial result.

In addition, different levels of model sophistication are explored, where it is shown that despite extreme simplifications, the minimalist model (with transmembrane protein, homogeneous lipid, and one-way coupling) has only ~20% difference with respect to the refined model. The analytical models, ECMM and ENM, which are based on the simplified interactions, are compared with MDeFEM simulation. The ECMM has imposed relevant bounds of the gating process, and the ENM can capture the structural evolutions during gating in a manner consistent with the MDeFEM simulations and the structural model (6). There are certain differences among different simulation protocols, which highlight the importance of specific components (e.g., the exposure of TM1 helices to lipid membrane) during gating. The ENM type of model can be made more sophisticated in terms of interactions among different components (24); with such improvements, the ENM-based approach can be used to develop structural transition models of other MS channels, similar in spirit to the pioneering work of Sukharev et al. for MscL (8), but in a more systematic fashion. An interesting application along this line is to compare the structural response of membrane proteins to various mechanical perturbations in the membrane.

To illustrate the MDeFEM framework's potential of handling large-scale problems, the refined model is applied to other loading modes and cooperativity of the channel. It is found that pure bending could only moderately increase the pore radius (if it is not coupled with in-plane tension), and uniaxial tension/in-plane shear/torsion are not effective gating mechanisms. The interaction between two neighboring *E. coli*-MscL (under equibiaxial tension) shows that the channels will influence each other if their center-to-center separation is below ~100 Å, or about four times the undeformed radius of lipid cavity, which agrees well with the simple analytical model derived in Part I of this study and literature (17). The sensitivity of MscL to particular mechanical perturbations has been implicitly assumed in previous work (5,25–27) and it has been shown explicitly using the MDeFEM approach.

To further demonstrate the ability of the MDeFEM framework to introduce complex deformation of the membrane, we simulate the gating characteristics of MscL when the surrounding membrane is subjected to a patch clamp or a nanoindentation ''experiment''. The former is extensively used in the experimental literature for MscL and related MS channels, although a quantitative interpretation of the result is not always straightforward. Nanoindentation is widely used in the engineering field to measure the mechanical properties of material structures at submicron scales and we probe its applicability to induce new gating behaviors in MscL. The versatile MDeFEM framework allows the simulation of laboratory experiments to guide and stimulate future experiments.

These studies not only reveal how different mechanical perturbations affect MS channels in potentially different ways, but also demonstrate the promising value of the top-down MDeFEM framework for analyzing mechanics-induced functional motions in biomolecules. Although there is still plenty of room for further improvement, the MDeFEM framework presented in this article captures the essential characteristics of the gating process, and the quantitative nature of the prediction can be improved as discussed in the section, ''Limitations of the current implementation''. We emphasize that no real-time dynamics information can be collected in the quasi-static simulations performed here. For that purpose, other extensions of the MDeFEM approach are necessary; interesting possibilities of immediate interest include considering temperature effects, which introduce thermal fluctuations into the gating process, and introducing time-dependent loading, which has been applied in many experiments to probe channel inactivation and desensitization (28). In addition, the effect of ions and charges on the mechanotransduction behaviors can be studied (29), as well as the transporting behavior of molecules through the channel

under external pressure (30–32). Through these systematic improvements, the top-down continuum-based strategy introduced here can be powerful for analyzing the gating transition of other MS channels and other biological processes where mechanical perturbation at large length (e.g., cellular) scales is important.

The work of Y.T. and X.C. is supported by National Science Foundation CMS-0407743 and CMMI-0643726. The work of J.Y. and Q.C. is supported by the National Institutes of Health (R01-GM071428-01). Q.C. also acknowledges a Research Fellowship from the Alfred P. Sloan Foundation. Computational resources from the National Center for Supercomputing Applications at the University of Illinois are greatly appreciated.

REFERENCES

1. Karplus, M., and J. Kuriyan. 2005. Molecular dynamics and protein function. *Proc. Natl. Acad. Sci. USA.* 102:6679–6685.
2. Hamill, O. P., and B. Martinac. 2001. Molecular basis of mechanotransduction in living cells. *Physiol. Rev.* 81:685–740.
3. Anishkin, A., and C. Kung. 2005. Microbial mechanosensation. *Curr. Opin. Neurol.* 15:397–405.
4. Kung, C. 2005. A possible unifying principle for mechanosensation. *Nature.* 436:647–654.
5. Gullingsrud, J., and K. Schulten. 2003. Gating of MscL studied by steered molecular dynamics. *Biophys. J.* 85:2087–2099.
6. Sukharev, S., and A. Anishkin. 2004. Mechanosensitive channels: what can we learn from 'simple' model systems? *Trends Neurosci.* 27:345–351.
7. Sukharev, S., P. Blount, B. Martinac, and C. Kung. 1997. Mechanosensitive channels of *Escherichia coli*: the MscL gene, protein and activities. *Annu. Rev. Physiol.* 59:633–657.
8. Sukharev, S., S. R. Durell, and H. R. Guy. 2001. Structural models of the MscL gating mechanism. *Biophys. J.* 61:917–936.
9. Tang, Y., G. Cao, X. Chen, J. Yoo, A. Yethiraj, and Q. Cui. 2006. A finite element framework for studying mechanical response of macromolecules: application to the gating of the mechanosensitive channel MscL. *Biophys. J.* 91:1248–1263.
10. Sukharev, S., W. J. Sigurdson, C. Kung, and F. Sachs. 1999. Energetic and spatial parameters for gating of the bacterial large conductance mechanosensitive channel, MscL. *J. Gen. Physiol.* 113:525–540.
11. Anishkin, A., C. S. Chiang, and S. Sukharev. 2005. Gain of function mutations reveal expanded intermediate states and a sequential action of two gates in MscL. *J. Gen. Physiol.* 125:155–170.
12. Yefimov, S. E. v. d. Giessen, P. R. Onck, and S. J. Marrink. 2008. Mechanosensitive membrane channels in action. *Biophys. J.* 94:2994–3002.
13. Perozo, E., A. Kloda, D. M. Cortes, and B. Martinac. 2002. Physical principles underlying the transduction of bilayer deformation forces during mechanosensitive channel gating. *Nat. Struct. Biol.* 9:696–703.
14. Meyer, G. R., J. Gullingsrud, K. Schulten, and B. Martinac. 2006. Molecular dynamics study of MscL interactions with a curved lipid bilayer. *Biophys. J.* 91:1630–1637.
15. Sukharev, S., M. Betanzos, C.-S. Chiang, and H. R. Guy. 2001. The gating mechanism of the large mechanosensitive channel MscL. *Nature.* 409:720–724.
16. Wiggins, P., and R. Philips. 2005. Membrane-protein interactions in mechanosensitive channels. *Biophys. J.* 88:880–902.
17. Ursell, T., K. C. Huang, E. Peterson, and R. Phillips. 2007. Cooperative gating and spatial organization of membrane proteins through elastic interactions. *PLoS Computational Biology.* 3:e81.
18. Chen, X., N. Ogasawara, M. Zhao, and N. Chiba. 2007. On the uniqueness of measuring elastoplastic properties from indentation: the indistinguishable mystical materials. *J. Mech. Phys. Solids.* 55:1618–1660.
19. Charras, G. T., and M. A. Horton. 2002. Single cell mechanotransduction and its modulation analyzed by atomic force microscope indentation. *Biophys. J.* 82:2970–2981.
20. Hartmann, C., and A. Delgado. 2004. Stress and strain in a yeast cell under high hydrostatic pressure. *PAMM.* 4:316–317.
21. Gordon, V., X. Chen, J. W. Hutchinson, A. R. Bausch, M. Marquez, and D. A. Weitz. 2004. Self-assembled inflated polymer membrane capsules. *J. Am. Chem. Soc.* 126:14117–14122.
22. Akitake, B., A. Anishkin, N. Liu, and S. Sukharev. 2007. Straightening and sequential buckling of the pore-lining helices define the gating cycle of MscS. *Nat. Struct. Biol.* 14:1141–1149.
23. Powl, A. M., and A. G. Lee. 2007. Lipid effects on mechanosensitive channels. *Curr. Top. Membr.* 58:151–178.
24. Moritsugu, K., and J. C. Smith. 2007. Coarse-grained biomolecular simulation with REACH: Realistic Extension Algorithm via Covariance Hessian. *Biophys. J.* 93:3460–3469.
25. Kong, Y., Y. Shen, T. E. Warth, and J. Ma. 2002. Conformational pathways in the gating of *Escherichia coli* mechanosensitive channel. *Proc. Natl. Acad. Sci. USA.* 99:5999–6004.
26. Turner, M. S., and P. Sens. 2004. Gating-by-tilt of mechanically sensitive membrane channels. *Phys. Rev. Lett.* 93:118103.
27. Phillips, R., M. Dittrich, and K. Schulten. 2002. Quasicontinuum representations of atomic-scale mechanics: from proteins to dislocations. *Annu. Rev. Mater. Res.* 32:219–233.
28. Morris, C. E., and P. F. Juranka. 2007. Lipid stress at play: mechanosensitivity of voltage-gated channels. *Curr. Top. Membr.* 59:297–338.
29. Liu, L., Y. Qiao, and X. Chen. 2008. Pressure-driven water infiltration into carbon nanotube: the effect of applied charges. *Appl. Phys. Lett.* 92:101927.
30. Qiao, Y., G. Cao, and X. Chen. 2007. Effect of gas molecules on nanofluidic behaviors. *J. Am. Chem. Soc.* 129:2355–2359.
31. Chen, X., F. B. Surani, X. Kong, V. K. Punyamurtula, and Y. Qiao. 2006. Energy absorption performance of a steel tube enhanced by a nanoporous material functionalized liquid. *Appl. Phys. Lett.* 89:241918.
32. Cao, G., Y. Qiao, and X. Chen. 2008. Infiltration behavior of water in a carbon nanotube under external pressure. *Phil. Mag. Lett.* 88:371–378.